



HAL
open science

Strain-induced magnetic moment variations at the picosecond timescale

C. Pfaff, T. Pezeril, R. Arras, L. Calmels, V. Cherruault, S. Andrieu, K. Dumesnil, J. Gorchon, T. Hauet

► **To cite this version:**

C. Pfaff, T. Pezeril, R. Arras, L. Calmels, V. Cherruault, et al.. Strain-induced magnetic moment variations at the picosecond timescale. *Physical Review B*, 2025, 111 (6), pp.064405. 10.1103/PhysRevB.111.064405 . hal-04927509

HAL Id: hal-04927509

<https://hal.science/hal-04927509v1>


Submitted on 5 Feb 2025

HAL is a multi-disciplinary open access archive for the deposit and dissemination of scientific research documents, whether they are published or not. The documents may come from teaching and research institutions in France or abroad, or from public or private research centers.

L'archive ouverte pluridisciplinaire **HAL**, est destinée au dépôt et à la diffusion de documents scientifiques de niveau recherche, publiés ou non, émanant des établissements d'enseignement et de recherche français ou étrangers, des laboratoires publics ou privés.



Distributed under a Creative Commons Attribution 4.0 International License

Strain-induced magnetic moment variations at the picosecond timescaleC. Pfaff,¹ T. Pezeril², R. Arras³, L. Calmels³, V. Cherruault², S. Andrieu¹,
K. Dumesnil¹, J. Gorchon¹ and T. Hauet¹¹Université de Lorraine, CNRS, IJL, F-54000 Nancy, France²Institut de Physique de Rennes, UMR CNRS 6251, Université de Rennes, 35042 Rennes, France³CEMES, Université de Toulouse, CNRS, 29 rue Jeanne Marvig, F-31055 Toulouse, France (Received 20 February 2024; revised 18 June 2024; accepted 17 January 2025; published 3 February 2025)

The spin-lattice interaction, a widely observed yet poorly understood phenomenon, has been often studied in the context of the coupling between lattice and magnetic anisotropies. It is also noteworthy that a quasistatic lattice compression is predicted to reduce the magnetic moment of pure ferromagnets such as cobalt and nickel. In this study, we utilize femtosecond laser pump/probe experiments to investigate the ability of a transient strain pulse to change the magnetic moment of a nanometric Co/Ni multilayer film at the picosecond timescale. In good agreement with static density functional theory calculations, our results reveal that a tensile strain acts oppositely to a compressive strain in increasing the magnetic moment, highlighting the efficiency of such magnetoelastic coupling at THz frequencies.

DOI: [10.1103/PhysRevB.111.064405](https://doi.org/10.1103/PhysRevB.111.064405)**I. INTRODUCTION**

The exploration of spin-lattice interaction dates back to the pioneering experimental observations of magnetostriction in an iron rod by Joule in 1842 [1]. Quasistatic change in magnetic anisotropy is the most common effect observed when a ferromagnet is coupled to quasistatic strain gauges [2], shape-alloy memory substrates [3], or piezoelectric substrates [4]. But lattice modification has also been predicted to impact the atomic magnetic moment itself [5–8]. A few synchrotron experiments using diamond anvil cell have indeed shown that a compression of the order of 1 to 100 GPa leads to a reduction of the *K*-edge x-ray magnetic dichroism signal for pure cobalt and nickel bulk samples, but this technique is sensitive to the *4p* orbital moment rather than to the total spin moment [8–11]. Extending these experimental results to a larger variety of samples and to tensile strain remains a challenge. Alternatively, femtosecond lasers have been used to trigger high frequency strain waves with GPa amplitudes [12,13] and study the resulting strain-induced magnetization dynamics over hundreds of picoseconds. Several studies have explored strain-induced magnetization precession [14–17] as well as the more exotic lattice-induced appearance of ferromagnetism in CoF₂ [18] and FeRh [19] antiferromagnets.

In this paper, we reveal subpicosecond enhancement (and reduction) of the magnetic moment attributed to tensile (and compressive) strain waves in epitaxial Co/Ni thin film ferromagnets. Magneto-optical Kerr (MOKE) measurements unveil ultrafast changes in the magnetization which coincide with the crossing of the acoustic pulses through the ferromagnetic layer. *Ab initio* calculations performed on Co/Ni systems provide consistent magnetic moment variations scaling with strain.

II. EXPERIMENTAL DETAILS

The samples are epitaxial heterostructures V(5 nm)/Au(15–20 nm)/Ni(0.6 nm)/[Co(*x*)/Ni(0.6 nm)]₅/MgO(90 nm) grown on a double side polished (11–20) Al₂O₃ single crystal substrate by molecular beam epitaxy under ultrahigh vacuum [see Fig. 1(a)]. We used the same growth process as developed in Refs. [20,21] and that we discuss in more detail in Supplemental Material Sec. 1 [22]. Following laser excitation of the stack, both the V and Co/Ni layers absorb part of the optical energy and generate unipolar acoustic pulses due to the fast lattice temperature changes [16,23–26]. Such strain pulses propagating along the *z* out-of-plane direction in the stack have been well studied in heterostructures via optical measurements [27] or (sub)picosecond hard x-ray diffraction [24,28], and are further described in Sec. 4 of the Supplemental Material [22]. Notably, the excellent acoustic impedance match between the Al₂O₃ substrate and the V, [Co/Ni], and MgO layers results in the generation of unipolar, purely compressive strain pulses propagating through the stack. This contrasts with scenarios involving a free surface, where strain pulses are bipolar, carrying tensile strain due to acoustic mismatches at the interface [29]. Additionally, strain pulses propagating laterally, primarily as surface acoustic waves on the nanosecond timescale and beyond, are excluded from our ultrafast study. Moreover, because of the low electron-phonon coupling in gold, the Au layer contribution to the acoustic wave excitation is negligible [30–32]. The insulating double side polished sapphire substrate and MgO layer are optically transparent. The Au and MgO layers only play the role of spacer in order to delay the arrival time of the acoustic pulses to the target layer (here Co/Ni) where the magnetoelastic interaction takes place. As discussed in Supplemental Material Sec. 3 [22], the use of anisotropic V (110) crystal plane and

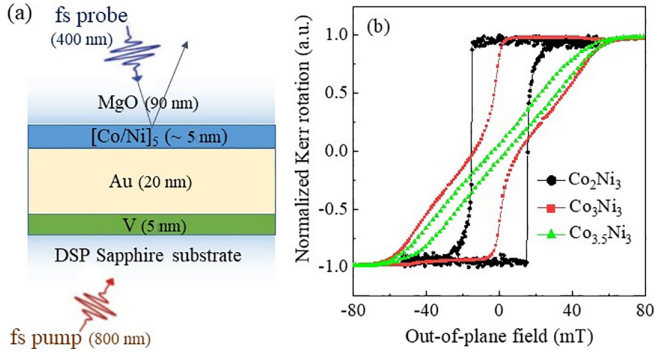


FIG. 1. (a) Scheme of the sample stack and the pump-probe experimental geometry. (b) Magneto-optical Kerr signal as a function of out-of-plane magnetic field amplitude measured at room temperature on Co_2Ni_3 , Co_3Ni_3 , and $\text{Co}_{3.5}\text{Ni}_3$ multilayer samples.

its birefringence properties offers us a method to probe the position of the strain pulses in the stack as a function of time after femtosecond laser pump pulse absorption. Finally, we chose Co/Ni multilayer as ferromagnetic layer because its perpendicular anisotropy can be tuned through the Co thickness [21,33,34] as well as for its relevance for future work on ultrafast spintronics [35,36]. Three $[\text{Co}(x)/\text{Ni}(0.6\text{nm})]_5$ multilayers, so-called Co_2Ni_3 , Co_3Ni_3 , $\text{Co}_{3.5}\text{Ni}_3$, were studied, having a Co thickness of 2 atomic monolayers (MLs) (i.e., 0.4 nm), 3, and 3.5 MLs respectively. Although all three multilayers carry perpendicular magnetic anisotropy, the overall anisotropy constant K_{eff} decreases from 0.35 MJ/m³ for Co_2Ni_3 to less than 0.1 MJ/m³ for $\text{Co}_{3.5}\text{Ni}_3$. Accordingly, magneto-optical Kerr rotation measured in polar geometry as a function of out-of-plane field amplitude shows, in Fig. 1(b), the continuous transition from a square hysteresis loop for Co_2Ni_3 with full magnetization at remanence to a tilted hysteresis for $\text{Co}_{3.5}\text{Ni}_3$ with an out-of-plane domain pattern at remanence [20,37].

All femtosecond pump-probe experiments were conducted at room temperature with an optical pump-probe setup based on a Ti:sapphire femtosecond laser outputting pulses of about 100 fs duration, at a repetition rate of 76 MHz, tuned to a central wavelength of 800 nm. The pump was focused onto the back side of the sample, across the double-side polished sapphire substrate, at a power of typically 380 mW (corresponding to a pump energy density of the order of 0.1 mJ/cm²). As a detection, we used a frequency-doubled probe (400 nm wavelength) at typically 4 mW power. The probe was tightly focused at normal incidence on the top sample surface. Additional information about the setup can be found in Sec. 2 of the Supplemental Material [22]. With this setup we have measured transient rotation of the polarization of the reflected probe beam, in polar geometry, as a function of time delay between pump and probe beams. In order to disentangle magnetic and nonmagnetic phenomena from the time-dependent polarization rotation signal $\Delta\theta_k$, each measurement was successively performed under two opposite fields or remanences $\Delta\theta_k(+H)$ and $\Delta\theta_k(-H)$. We define as the MOKE component the term $0.5[\Delta\theta_k(+H) - \Delta\theta_k(-H)]$ which should be sensitive only to magneto-optics. The field independent signal, referred to as FIS, is de-

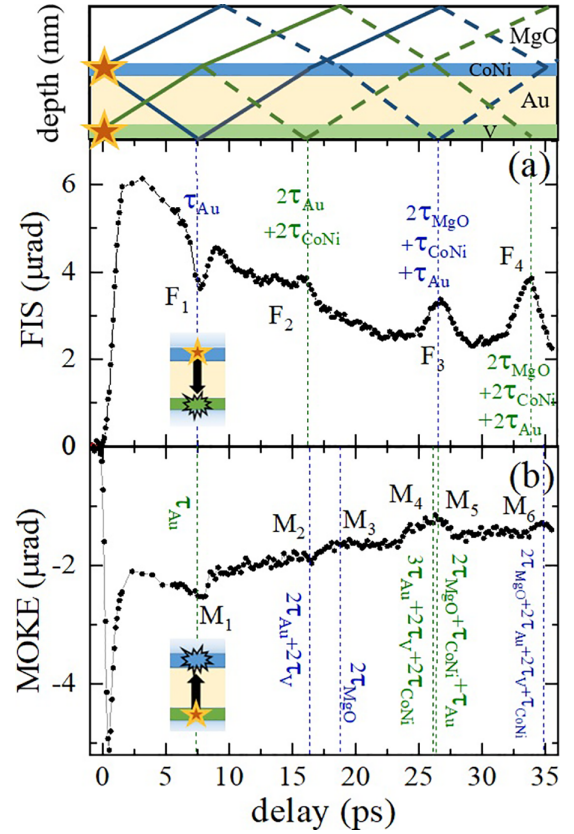


FIG. 2. Field-independent signal (FIS) signal (a) and MOKE signal (b) measured on a Co_2Ni_3 sample under ± 80 mT. Series of F and M peaks occur when strain waves hit the vanadium layer and the Co/Ni layer respectively, as shown in the top scheme. In this scheme, the full lines indicate compressive strain waves and the dotted lines the tensile strain waves while the green (respectively blue) lines indicate the strain wave originating from the laser pumping in V (respectively in Co/Ni). The scheme in (a) [respectively in (b)] shows that the FIS (respectively MOKE) peak at 7.5 ps originates from the pump-induced compressive strain wave propagating from Co/Ni to V (respectively from V to Co/Ni).

fined as $0.5[\Delta\theta_k(+H) + \Delta\theta_k(-H)]$, which is both sensitive to reflectivity changes and linear optical anisotropies (e.g., birefringence).

III. RESULTS AND DISCUSSION

First, we highlight the production and propagation of unipolar strain waves through the sample depth using the FIS signal measured on the Co_2Ni_3 sample shown in Fig. 2(a). As explained in Supplemental Material Sec. 3 [22], the FIS signal originates solely from the linear optical birefringence from the anisotropic V (110) layer [38–40]. Two main features are observed in Fig. 2(a): a step signal which saturates around 2 ps and then slowly decreases at larger time, and four peaks which occur at around 7.5, 17, 26.5, and 34 ± 0.5 ps respectively. The positive step signal comes from the expansion of the V layer when absorbing the pump energy. The peak F_1 occurs at a time, named τ_{Au} , of 7.5 ps after the pump excites the sample and corresponds to the time required for the acoustic pulse excited in Co/Ni to travel across the 20-nm gold layer at a speed

of sound in Au of 3300 m/s before entering the V layer where it is detected through the FIS signal. The smaller peak F_2 in Fig. 2(a) occurs at about 17 ps, indicated as $2\tau_{\text{Au}} + 2\tau_{\text{Co/Ni}}$ and is consistent with the acoustic echo excited in the vanadium layer that has traveled back and forth through the gold layer due to the reflection at the [Co/Ni]/MgO interface. The speed of sound in V being of about 4500 m/s, and in Co/Ni of about 6000 m/s, the travel time of the acoustic wave in V and Co/Ni layers is about 1 ps. In Supplemental Material Sec. 4 [22], we present a table for speed of sound in the various layer as well as the calculations of the strain reflection R and transmission T coefficients across each interface from the acoustic mismatch model [41]. The reflection coefficient at the [Co/Ni]/MgO interface is calculated to be negative so that the acoustic wave switches from a compressive to a tensile strain after reflection on this interface, in good agreement with previous reports [25]. As a consequence, the sign of the F_2 peak is the same as the step signal but opposite to the F_1 peak's one. F_3 and F_4 peaks refer to the acoustic echo laser excited in Co/Ni, respectively V, which has traveled back and forth through the 90-nm MgO layer at a speed of sound of 9100 m/s and interacts in the vanadium layer at $2\tau_{\text{MgO}} + \tau_{\text{Au}} + \tau_{\text{Co/Ni}}$, respectively $2\tau_{\text{MgO}} + 2\tau_{\text{Au}} + 2\tau_{\text{Co/Ni}}$. Their sign is opposite to F_1 because of the negative reflection coefficient at the MgO/air interface. The amplitudes of F_1 and F_3 , both related to the Co/Ni-induced strain pulse, are similar because the acoustic reflection coefficient at the MgO/air interface is -1 . On the contrary the amplitude of F_2 is only a fourth of the F_4 , although both are related to V-induced strain pulses, due to the smaller reflection at the [Co/Ni]/MgO interface (-0.25). The comparison of the FIS peak's amplitudes also confirms that the transient strain produced by V is larger than the one produced by Co/Ni, consistently with a back-side pump excitation through the sapphire substrate that drives more energy into V than into Co/Ni. At this stage, we can conclude that laser pump pulses produce strain waves in the V and Co/Ni layers. These ultrashort strain pulses of about 1 ps in duration can be detected through FIS from birefringence of the V(110) crystalline layer. One can get rid of the FIS signal by using stacks involving a thicker gold film for which the probe light does not optically penetrate into the V layer (as outlined in Supplemental Material Sec. 3 [22]).

Figure 2(b) shows time-resolved MOKE data obtained by subtracting the polarization rotation amplitudes under $+80$ mT and -80 mT. In less than 0.5 ps after the pump excites the sample, an ultrafast discontinuity in the MOKE amplitude happens due to the ultrafast heating and immediate partial demagnetization of the Co/Ni multilayer [42,43]. This sudden fall is followed by a slow remagnetization towards the saturated state. The amplitude of the demagnetization peak is around 1% of the full saturation Kerr rotation. It indicates that the laser-induced temperature rise is well below the Curie temperature and thus Co/Ni can still be considered close to its equilibrium ferromagnetic state [44]. It agrees with the calculation of the absorption profile and the corresponding temperature increase of only a few K produced by a laser excitation with a fluence of 0.1 mJ/cm². Interestingly, at around 7.5 ps, a second MOKE peak (M_1) is detected which takes place simultaneously to the compressive strain pulse detected in V through the FIS signal in Fig. 2(a). Indeed, as discussed

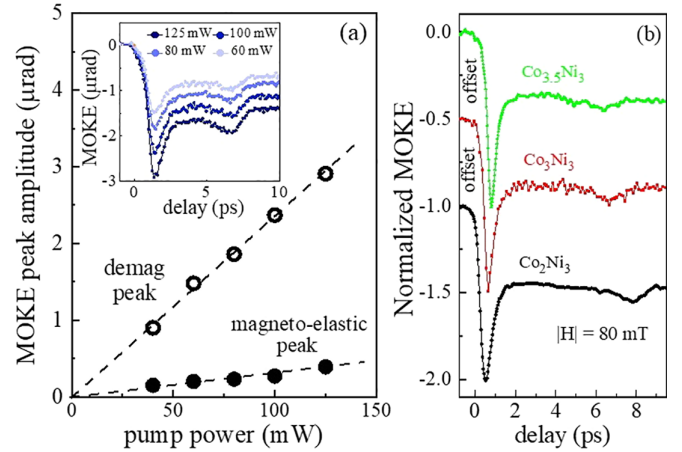


FIG. 3. (a) Demagnetization peak and strain-induced (so-called magnetoelastic) peak amplitudes extracted from time-resolved MOKE spectra on a Co_2Ni_3 sample, as a function of pump power. In inset, series of time-resolved MOKE spectra obtained for different pump powers. (b) Normalized MOKE signal measured successively on three Co_xNi_3 samples with $x = 2, 3$, and 3.5 monolayers, respectively, under 80-mT magnetic field at 380-mW pump power.

earlier, the pump laser induces both a strain wave in Co/Ni which travels across Au and reaches V at τ_{Au} and a strain wave in V that travels across Au and reaches Co/Ni at τ_{Au} as well. The amplitude of this strain-induced MOKE peak is about $8 \pm 0.5\%$ of the demagnetization MOKE peak amplitude (i.e., 0.08% of the saturation magnetization). In Fig. 3(a), the amplitudes of the demagnetization and M_1 peaks are found to rise linearly with the pump power. So, transferring more laser power to the vanadium intensifies the strain wave amplitude and consequently enhances the strain-induced MOKE peaks. Five additional MOKE peaks are seen in Fig. 2(b). The sign of M_2 occurring at $2\tau_{\text{Au}} + 2\tau_{\text{V}}$ is identical to the sign of M_1 because it originates from the strain wave produced in Co/Ni and reflected at the V/ Al_2O_3 interface with a positive acoustic reflection coefficient (see Supplemental Material Sec. 4 [22]). The next positive MOKE peaks, M_3 to M_6 , correspond to the coupling between Co/Ni and the strain waves transformed into tensile after full acoustic reflection at the MgO/air interface. The amplitude of the peaks M_2 , M_3 and M_6 are smaller than the two others because they relate to the Co/Ni-induced strain pulse. The peak M_2 is even much smaller than the other ones because the acoustic reflection coefficient at V/ Al_2O_3 is calculated to be only $+0.19$, so the strain amplitude coming back to Co/Ni after this reflection is much reduced. Additionally, as shown in Sec. 5 of the Supplemental Material [22], the amplitude of the magnetoelastic peaks monotonically decreases when the Co/Ni layer moment is partially reversed during minor loops, and becomes null when the sample contains half up and half down magnetized domains. These data also confirm that the laser fluence of ~ 0.1 mJ/cm² is so small that it can only slightly perturb the magnetic state, and therefore the system always naturally recovers its prepump magnetic state. Given the nature of MOKE [45], we can now safely assert that the observed MOKE peaks, apart from the demagnetization one, are the result of changes in either the optical constant

and/or magnetic properties of the samples, due to the acoustic pulses.

As the M_1 to M_6 peaks are concomitant with the acoustic pulses reaching the Co/Ni layer, any magneto-optical artefacts that would involve an acoustic modification of the optical indices in the surrounding layers can be excluded (e.g., Brillouin oscillations [17]). Besides, the magneto-optical constants of the ferromagnetic layer themselves should remain unchanged in the used fluence range (particularly for time delays of 1 ps and above), as previously verified in Co_3Pt [46], Ni [47], or in TbFe_2 [24], and as assumed by almost all the literature works using time-resolved MOKE. Only in GaMnAsP , a strain-induced MOKE signal was explained by the strain pulse's modulation of the reflectivity instead of a magnetization change [48]. As a matter of fact, we did not record any significant variation of reflectivity when the strain pulses cross the Co/Ni layer (see Fig. S5 [22]). Therefore, even if the sensitivity of our reflectivity measurement method may have been improved by balancing the signal with a reference beam, the decent signal-to-noise ratio allows us to conclude that, if any, the modification of the reflectivity by the strain pulse in Co/Ni is small contrary to the MOKE variation. Finally, based on the above discussion, we attribute the MOKE peaks M_1 to M_6 , which are referred to as magnetoelastic peaks in the following, to either a change of amplitude or direction of the Co/Ni magnetic moment, and not to a change of complex refractive index. In our previous work on TbFe_2 [24], we could not disentangle the possible sources of strain-induced MOKE change because of the complex magnetic microstructure of TbFe_2 , its in-plane anisotropy, and the strong saturation field. Here the uniaxial out-of-plane anisotropy and the low saturation field of Co/Ni make it possible to specifically reveal the strain-induced change of the magnetization amplitude.

We use the well-known dependence of magnetic anisotropy of Co/Ni multilayers on Co thickness [21,33,34] to check its influence on the magnetoelastic peaks. Figure 3(b) presents the time-dependent MOKE signals collected in Co_2Ni_3 , Co_3Ni_3 , and $\text{Co}_{3.5}\text{Ni}_3$ samples. The same features are observed for the three samples with a demagnetization peak at a time below 1 ps and a first strain-induced peak at a time ranging 6.4–7.7 ps. The variability in the time of occurrence of the magnetoelastic peak is due to deviations from the nominal gold thickness, as described in more detail in Supplemental Material Sec. 1 [22]. The magnetoelastic peak amplitude for Co_3Ni_3 is $0.075 \pm 0.005\%$ of the saturated moment, hardly distinguished from the Co_2Ni_3 one ($0.08 \pm 0.005\%$), while the amplitude is further reduced down to $0.065 \pm 0.005\%$ for $\text{Co}_{3.5}\text{Ni}_3$. A transient reduction of anisotropy is expected to promote a much more dramatic moment rotation towards the film plane, so a much larger MOKE variation, in $\text{Co}_{3.5}\text{Ni}_3$ having the smallest K_{eff} (near the out-of-plane to in-plane anisotropy transition). It is not what we observe experimentally. Moreover, a transient reduction of the anisotropy due to the laser pulse or to the laser induced strain pulse, and a subsequent change of moment direction, must trigger precession or variation of the precession of the magnetization at GHz frequency [14–17]. In the present samples, such a precession is only laser-induced when an additional in-plane external field is applied [see Figs. S4(b) and S4(c) of the Supplemental Material [22]], in agreement with previous reports

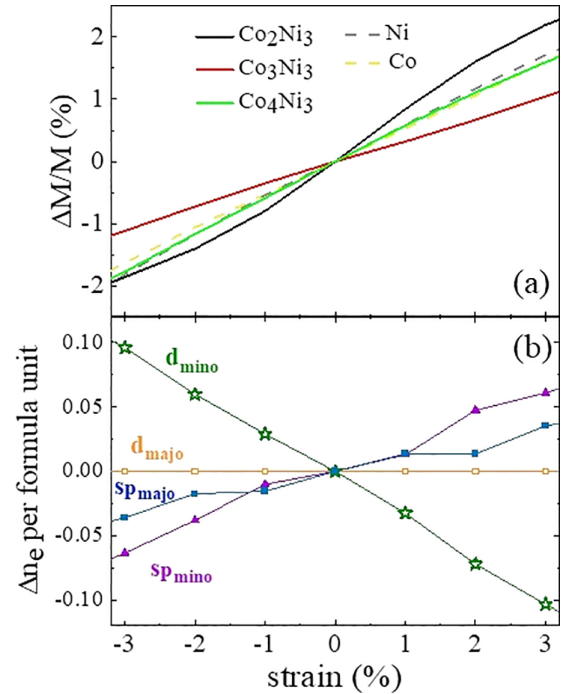


FIG. 4. (a) Theoretical relative variation of moment as a function of the strain applied along the z axis, perpendicular to the stacking of three Co_xNi_3 samples, compared with pure Co(111) and pure Ni(111). (b) Variation of the number of majority (majo) and minority (mino) spin electron of s - p and d type, calculated from the integrated DOS of the Co_2Ni_3 superlattice as a function of the applied strain.

[49]. MOKE oscillations occur over a much larger timescale than the picosecond-wide magnetoelastic peaks. Therefore, we conclude that the magnetoelastic peaks observed in our experiments originate from a modification of the value of the magnetic moment itself, similar to the quasistatic reduction of the moment induced by a compression in a diamond anvil cell [8–11].

First-principles calculations based on the density functional theory (DFT) have been performed using the VASP code [50,51] (more details are given in Supplemental Material Sec. 7 [22]). The variations of magnetic moments, including the spin and orbital contributions, have been calculated by applying strain only along the out-of-plane direction. The in-plane lattice parameters are kept to their unchanged equilibrium value to mimic the femtosecond laser induced strain pulse [52]. The moment of Co_xNi_3 is calculated to increase linearly when the lattice is stretched along the z axis, in good agreement with our findings in Fig. 2(b). Based on the DFT data in Fig. 4(a), the experimental $\Delta M/M$ of 0.08% in Co_2Ni_3 (extracted from Figs. 2 and 3) should originate from a strain of the order of 0.1%. This value of 0.1% is approximately 20 times larger than the maximum strain calculated in considering a maximum temperature increase of 10 K (due to the absorbed optical energy density of 0.1 mJ/cm^2) and the linear thermal expansion coefficient of about 10^{-6} K^{-1} in V and Co/Ni layers. A more sophisticated calculation was undertaken using the `udkm1Dsim` toolbox package [53] to determine the spatiotemporal strain map in our multilayer system. It reveals that the maximum strain which propagates in

the V/Au/Co/Ni/MgO stack after laser absorption is indeed of the order of $\pm 0.5 \times 10^{-4}$ (see Supplemental Material Sec. 8 [22]). The difference of one order of magnitude between DFT and MOKE measurements remains puzzling but the drastic approximation for DFT calculations could be an explanation. It is to be noted that both sign and amplitude of the moment variation calculated by DFT here agree with previous DFT calculation reports characterizing the reduction of magnetic moment with volume compression of pure Co and Ni [5–8]. But, interestingly, no direct experimental characterization of the magnetic moment change is available in the literature (only $4p$ orbital moment variation under strain has been collected). Besides, experimental demonstration of strain-wave induced modulation of the MOKE in pure Co and Ni seems absent from the literature [54]. A few reasons can explain it. Pure Co and Ni have in-plane anisotropy and it is well established that longitudinal MOKE has a lower sensitivity than polar MOKE used for system with perpendicular anisotropy. The Kerr geometry may have been a limitation for pure Co and Ni, whereas this magnetoacoustic effect is clearly demonstrated for pure Ni and Co crystals in XMCD measurements under pressure. Besides, the generation of a unipolar strain at the sapphire/V and Co/Ni/MgO interfaces is a specificity in our experiments that avoids strain averaging effects present in previous works. Finally, the absence of controlled delay time between the light energy arrival (and so the demagnetization process) and the acoustic wave arrival in previous femtosecond laser experiments on pure Co and Ni may have hidden the magnetoacoustic process calculated in Fig. 4.

Finally, allowing the lateral dimension of the lattice to relax does not modify the overall DFT calculation results (see Supplemental Material Sec. 7 [22]): data calculated with the relaxed and nonrelaxed superlattice cells superpose to each other when the moment variation is plotted as a function of the total volume. It confirms that the main ingredient to observe a compression-induced reduction or a tension-induced enhancement of the magnetic moment is the change in the atomic cell

volume. In Fig. 4(b), the density of states (DOS) integrated up to the Fermi level is found to decrease when the lattice volume expands for the minority spin d electrons, while it remains constant for the majority spin d electrons. In the same time, the integrated density of states for majority and minority spin s - p electrons grow. Such a transfer of the electronic density from the minority spin d bands to both the majority and minority spin s - p bands when the lattice is stretched explains the positive slope of $\Delta M/M$ vs strain as depicted in Fig. 4(a).

IV. SUMMARY

In conclusion, we have used femtosecond laser pulses to laser excite ultrashort strain waves in a sapphire/V/Au/[Co/Ni]₅/MgO stack. We have shown that these ultrashort strain pulses interact with and affect the net magnetization of the Co/Ni multilayers. Along with *ab initio* calculations, our experiments unveil the ability to controllably increase or decrease the moment of a ferromagnetic layer at the picosecond timescale with a transient strain pulse. Owing to the facts that ultrafast strain acoustic waves can be laser excited nondestructively with amplitudes reaching 1% (corresponding to pressures of a couple of GPa, i.e., more than ten times larger than the strain amplitudes produced here) in a similar sample geometry [12,13], and that our methodology allows us to combine MOKE, L -edge XMCD, and hard x-ray diffraction characterization, our present results pave the way to deeper understanding and control of ultrafast response of a wide range of magnetic materials to both extreme compression and tension.

ACKNOWLEDGMENTS

We acknowledge insightful discussions with L. Thevenard regarding our experimental results. Funding for this project was provided by ANR Ultramox under Grant No. ANR-14-CE26-0008. This work was performed using HPC resources from CALMIP (Grant No. 2023/2024-[P20042]).

-
- [1] M. Foerster and F. Macià, Preface to special issue on magneto-elastic effects, *J. Phys.: Condens. Matter* **31**, 190301 (2019).
 - [2] S. Nakagawa, M. Yamada, and N. Tokuriki, Stress induced enhancement of magnetization reversal process of DyFeCo films with perpendicular magnetization, *IEEE Trans. Magn.* **42**, 3773 (2006).
 - [3] A. Kyianytsia, M. Pongot, A. Letoffe, P. Boulet, S. Migot, J. Ghanbaja, I. Cinar, R. Lima de Miranda, C. Bechtold, B. Kierren, O. Ozatay, and T. Hauet, Magnetic anisotropy switching induced by shape memory effect in NiTi/Ni bilayer, *Appl. Phys. Lett.* **115**, 222402 (2019).
 - [4] V. Novosad, Y. Otani, A. Ohsawa, S. G. Kim, K. Fukamichi, J. Koike, K. Maruyama, O. Kitakami, and Y. Shimada, Novel magnetostrictive memory device, *J. Appl. Phys.* **87**, 6400 (2000).
 - [5] T. Jarlborg, Spin fluctuations, electron–phonon coupling and superconductivity in near-magnetic elementary metals—Fe, Co, Ni and Pd, *Physica C: Superconduct.* **385**, 513 (2003).
 - [6] P. Modak, A. K. Verma, R. S. Rao, B. K. Godwal, and R. Jeanloz, *Ab initio* total-energy and phonon calculations of Co at high pressures, *Phys. Rev. B* **74**, 012103 (2006).
 - [7] G. Steinle-Neumann, Magneto-elastic effects in compressed cobalt from first-principle, *Phys. Rev. B* **77**, 104109 (2008).
 - [8] R. Torchio, C. Marini, Y. O. Kvashnin, I. Kantor, O. Mathon, G. Garbarino, C. Meneghini, S. Anzellini, F. Occelli, P. Bruno, A. Dewaele, and S. Pascarelli, Structure and magnetism of cobalt at high pressure and low temperature, *Phys. Rev. B* **94**, 024429 (2016), and cited references.
 - [9] V. Iota, J.-H. Park Klepeis, C.-S. Yoo, J. Lang, D. Haskell, and G. Srajer, Electronic structure and magnetism in compressed transition metals, *Appl. Phys. Lett.* **90**, 042505 (2007).
 - [10] R. Torchio, Y. O. Kvashnin, S. Pascarelli, O. Mathon, C. Marini, L. Genovese, P. Bruno, G. Garbarino, A. Dewaele, F. Occelli, and P. Loubeyre, X-Ray magnetic circular dichroism measurements in Ni up to 200 GPa: Resistant ferromagnetism, *Phys. Rev. Lett.* **107**, 237202 (2011).

- [11] R. Torchio, A. Monza, F. Baudelet, S. Pascarelli, O. Mathon, E. Pugh, D. Antonangeli, and J. Paul Itié, Pressure-induced collapse of ferromagnetism in cobalt up to 120 GPa as seen via x-ray magnetic circular dichroism, *Phys. Rev. B* **84**, 060403(R) (2011).
- [12] V. V. Temnov, C. Klieber, K. A. Nelson, T. Thomay, V. Knittel, A. Leitenstorfer, D. Makarov, M. Albrecht, and R. Bratschitsch, Femtosecond nonlinear ultrasonics in gold probed with ultrashort surface plasmons, *Nat. Commun.* **4**, 1468 (2013).
- [13] T. Pezeril, C. Klieber, V. Shalagatskyi, G. Vaudel, V. Temnov, O. G. Schmidt, and D. Makarov, Femtosecond imaging of nonlinear acoustics in gold, *Opt. Express* **22**, 4590 (2014).
- [14] J.-W. Kim, M. Vomir, and J.-Y. Bigot, Ultrafast magnetoacoustics in nickel films, *Phys. Rev. Lett.* **109**, 166601 (2012).
- [15] A. V. Scherbakov, A. S. Salasyuk, A. V. Akimov, X. Liu, M. Bombeck, C. Brüggemann, D. R. Yakovlev, V. F. Sapega, J. K. Furdyna, and M. Bayer, Coherent magnetization precession in ferromagnetic (Ga,Mn)As induced by picosecond acoustic pulses, *Phys. Rev. Lett.* **105**, 117204 (2010).
- [16] J. V. Jäger, A. V. Scherbakov, T. L. Linnik, D. R. Yakovlev, M. Wang, P. Wadley, V. Holy, S. A. Cavill, A. V. Akimov, A. W. Rushforth, and M. Bayer, Picosecond inverse magnetostriction in galfenol thin films, *Appl. Phys. Lett.* **103**, 032409 (2013).
- [17] M. Deb, E. Popova, M. Hehn, N. Keller, S. Mangin, and G. Malinowski, Picosecond acoustic-excitation-driven ultrafast magnetization dynamics in dielectric Bi-substituted yttrium iron garnet, *Phys. Rev. B* **98**, 174407 (2018).
- [18] A. S. Disa, M. Fechner, T. F. Nova, B. Liu, M. Först, D. Prabhakaran, P. G. Radaelli, and A. Cavalleri, Polarizing an antiferromagnet by optical engineering of the crystal field, *Nat. Phys.* **16**, 937 (2020).
- [19] S. O. Mariager, F. Pressacco, G. Ingold, A. Caviezel, E. Mohr-Vorobeva, P. Beaud, S. L. Johnson, C. J. Milne, E. Mancini, S. Moyerman, E. E. Fullerton, R. Feidenhansl, C. H. Back, and C. Quitmann, Structural and magnetic dynamics of a laser induced phase transition in FeRh, *Phys. Rev. Lett.* **108**, 087201 (2012).
- [20] S. Girod, M. Gottwald, S. Andrieu, S. Mangin, J. McCord, E. E. Fullerton, J.-M. L. Beaujour, B. J. Krishnatreya, and A. D. Kent, Strong perpendicular magnetic anisotropy in Ni/Co(111) single crystal superlattices, *Appl. Phys. Lett.* **94**, 262504 (2009).
- [21] M. Gottwald, S. Andrieu, F. Gimbert, E. Shipton, L. Calmels, C. Magen, E. Snoeck, M. Liberati, T. Hauet, E. Arenholz, S. Mangin, and E. E. Fullerton, Co/Ni(111) superlattices studied by microscopy, x-ray absorption, and *ab initio* calculations, *Phys. Rev. B* **86**, 014425 (2012).
- [22] See Supplemental Material at <http://link.aps.org/supplemental/10.1103/PhysRevB.111.064405> for sample growth, structural and magnetic details; femtosecond pump-probe experiments, technical details; influence of optical birefringence on the field-independent polarization rotation; acoustic waves production and propagation; MOKE signal with Co/Ni magnetic domain configuration or in-plane field; reflectivity measurement; details on the first-principles calculations; strain amplitude and strain propagation calculations with udkm1Dsim toolbox package, which also contains Refs. [55–57].
- [23] T. Saito, O. Matsuda, and O. B. Wright, Picosecond acoustic phonon pulse generation in nickel and chromium, *Phys. Rev. B* **67**, 205421 (2003).
- [24] S. P. Zeuschner, T. Parpiiev, T. Pezeril, A. Hillion, K. Dumesnil, A. Anane, J. Pudell, L. Willig, M. Rössle, M. Herzog, A. von Reppert, and M. Bargheer, Tracking picosecond strain pulses in heterostructures that exhibit giant magnetostriction, *Struct. Dyn.* **6**, 024302 (2019).
- [25] W. Zhang, P. Maldonado, Z. Jin, T. S. Seifert, J. Arabski, G. Schmerber, E. Beaurepaire, M. Bonn, T. Kampfrath, P. M. Oppeneer, and D. Turchinovich, Ultrafast terahertz magnetometry, *Nat. Commun.* **11**, 4247 (2020).
- [26] A. von Reppert, M. Mattern, J.-E. Pudell, S. P. Zeuschner, K. Dumesnil, and M. Bargheer, Unconventional picosecond strain pulses resulting from the saturation of magnetic stress within a photoexcited rare earth layer, *Struct. Dyn.* **7**, 024303 (2020).
- [27] C. Klieber, V. E. Gusev, T. Pezeril, and K. A. Nelson, Nonlinear acoustics at GHz frequencies in a viscoelastic fragile glass former, *Phys. Rev. Lett.* **114**, 065701 (2015).
- [28] D. A. Reis, M. F. DeCamp, P. H. Bucksbaum, R. Clarke, E. Dufresne, M. Hertlein, R. Merlin, R. Falcone, H. Kapteyn, M. M. Murnane, J. Larsson, Th. Missalla, and J. S. Wark, Probing impulsive strain propagation with x-ray pulses, *Phys. Rev. Lett.* **86**, 3072 (2001).
- [29] M. Mattern, A. von Reppert, S. Peer Zeuschner, M. Herzog, J.-E. Pudell, and M. Bargheer, Concepts and use cases for picosecond ultrasonics with x-rays, *Photoacoustics* **31**, 100503 (2023).
- [30] A. Schenlohr, M. Battiato, P. Maldonado, N. Pontius, T. Kachel, K. Holldack, R. Mitzner, A. Föhlisch, P. M. Oppeneer, and C. Stamm, Ultrafast spin transport as key to femtosecond demagnetization, *Nat. Mater.* **12**, 332 (2013).
- [31] M. Lejman, V. Shalagatskyi, O. Kovalenko, T. Pezeril, V. V. Temnov, and P. Ruello, Ultrafast optical detection of coherent acoustic phonons emission driven by superdiffusive hot electrons, *J. Opt. Soc. Am. B* **31**, 282 (2014).
- [32] N. Berggaard, M. Hehn, S. Mangin, G. Lengaigne, F. Montaigne, M. L. M. Lalieu, B. Koopmans, and G. Malinowski, Hot-electron-induced ultrafast demagnetization in Co/Pt multilayers, *Phys. Rev. Lett.* **117**, 147203 (2016).
- [33] G. H. O. Daalderop, P. J. Kelly, and F. J. A. den Broeder, Prediction and confirmation of perpendicular magnetic anisotropy in Co/Ni multilayers, *Phys. Rev. Lett.* **68**, 682 (1992).
- [34] S. Andrieu, T. Hauet, M. Gottwald, A. Rajanikanth, L. Calmels, A. M. Bataille, F. Montaigne, S. Mangin, E. Otero, P. Ohresser, P. Le Fèvre, F. Bertran, A. Resta, A. Vlad, A. Coati, and Y. Garreau, Co/Ni multilayers for spintronics: High spin polarization and tunable magnetic anisotropy, *Phys. Rev. Mater.* **2**, 064410 (2018).
- [35] S. Mangin, D. Ravelosona, J. A. Katine, M. J. Carey, B. D. Terris, and Eric E. Fullerton, Current-induced magnetization reversal in nanopillars with perpendicular anisotropy, *Nat. Mater.* **5**, 210 (2006).
- [36] A. J. Schellekens, K. C. Kuiper, R. R. J. C. de Wit, and B. Koopmans, Ultrafast spin-transfer torque driven by femtosecond pulsed-laser excitation, *Nat. Commun.* **5**, 4333 (2014).
- [37] O. Hellwig, A. Berger, J. B. Kortright, and E. E. Fullerton, Domain structure and magnetization reversal of antiferromagnetically coupled perpendicular anisotropy films, *J. Magn. Mater.* **319**, 13 (2007).
- [38] M. Lejman, G. Vaudel, I. C. Infante, I. Chaban, T. Pezeril, M. Edely, G. F. Nataf, M. Guennou, J. Kreisel, V. E. Gusev, B. Dkhil, and P. Ruello, Ultrafast acousto-optic mode conversion in optically birefringent ferroelectrics, *Nat. Commun.* **7**, 12345 (2016).

- [39] J. John, A. Slassi, J. Sun, Y. Sun, R. Bachelet, J. Pénuelas, G. Saint-Girons, R. Orobtcouk, S. Ramanathan, A. Calzolari, and S. Cueff, Tunable optical anisotropy in epitaxial phase-change VO₂ thin films, *Nanophotonics* **11**, 3913 (2022).
- [40] T. Pezeril, P. Ruello, S. Gougeon, N. Chigarev, D. Mounier, J.-M. Breteau, P. Picart, and V. Gusev, Generation and detection of plane coherent shear picosecond acoustic pulses by lasers: Experiment and theory, *Phys. Rev. B* **75**, 174307 (2007).
- [41] O. Kovalenko, T. Pezeril, and V. V. Temnov, New concept for magnetization switching by ultrafast acoustic pulses, *Phys. Rev. Lett.* **110**, 266602 (2013).
- [42] E. Beaupaire, J.-C. Merle, A. Daunois, and J.-Y. Bigot, Ultrafast spin dynamics in ferromagnetic nickel, *Phys. Rev. Lett.* **76**, 4250 (1996).
- [43] C. Stamm, T. Kachel, N. Pontius, R. Mitzner, T. Quast, K. Hollmack, S. Khan, C. Lupulescu, E. F. Aziz, M. Wietstruk, H. A. Dürr, and W. Eberhardt, Femtosecond modification of electron localization and transfer of angular momentum in nickel, *Nat. Mater.* **6**, 740 (2007).
- [44] J. Hohlfeld, S.-S. Wellershoff, J. Güdde, U. Conrad, V. Jahnke, and E. Matthias, Electron and lattice dynamics following optical excitation of metals, *Chem. Phys.* **251**, 237 (2000).
- [45] J. Hamrle, Magneto-optical determination of the in-depth magnetization profile in magnetic multilayers, Ph.D. thesis (Université Paris XI and Charles University, Praha, 2003).
- [46] J.-Y. Bigot, L. Guidoni, E. Beaupaire, and P. N. Saeta, Femtosecond spectrotemporal magneto-optics, *Phys. Rev. Lett.* **93**, 077401 (2004).
- [47] B. Koopmans, M. van Kampen, J. T. Kohlhepp, and W. J. M. de Jonge, Ultrafast magneto-optics in nickel: Magnetism or optics? *Phys. Rev. Lett.* **85**, 844 (2000).
- [48] L. Thevenard, E. Peronne, C. Gourdon, C. Testelin, M. Cubukcu, E. Charron, S. Vincent, A. Lemaître, and B. Perrin, Effect of picosecond strain pulses on thin layers of the ferromagnetic semiconductor (Ga,Mn)(As,P), *Phys. Rev. B* **82**, 104422 (2010).
- [49] J. Jarecki, M. Mattern, F.-C. Weber, J.-E. Pudell, X.-G. Wang, J.-C. Rojas Sanchez, M. Hehn, A. von Reppert, and M. Bargheer, Controlling effective field contributions to laser-induced magnetization precession by heterostructure design, *Commun. Phys.* **7**, 112 (2024).
- [50] G. Kresse and J. Hafner, *Ab initio* molecular-dynamics simulation of the liquid-metal–amorphous–semiconductor transition in germanium, *Phys. Rev. B* **49**, 14251 (1994).
- [51] G. Kresse and J. Furthmüller, Efficient iterative schemes for *ab initio* total-energy calculations using a plane-wave basis set, *Phys. Rev. B* **54**, 11169 (1996).
- [52] M.-C. Lee, N. Sirica, S. W. Teitelbaum, A. Maznev, T. Pezeril, R. Tutchton, V. Krapivin, G. A. de la Pena, Y. Huang, L. X. Zhao, G. F. Chen, B. Xu, R. Yang, J. Shi, J.-X. Zhu, D. A. Yarotski, X. G. Qiu, K. A. Nelson, M. Trigo, D. A. Reis, and R. P. Prasankumar, Direct observation of coherent longitudinal and shear acoustic phonons in TaAs using ultrafast x-ray diffraction, *Phys. Rev. Lett.* **128**, 155301 (2022).
- [53] D. Schick, UDKM1DSIM – a Python toolbox for simulating 1D ultrafast dynamics in condensed matter, *Comput. Phys. Commun.* **266**, 108031 (2021).
- [54] M. Borchert, C. von Korff Schmising, D. Schick, D. Engel, S. Sharma, S. Shallcross, and S. Eisebitt, Uncovering the role of the density of states in controlling ultrafast spin dynamics, [arXiv:2008.12612](https://arxiv.org/abs/2008.12612).
- [55] T. Kato, Y. Matsumoto, S. Okamoto, N. Kikuchi, O. Kitakami, N. Nishizawa, S. Tsunashima, and S. Iwata, Time-resolved magnetization dynamics and damping constant of sputtered Co/Ni multilayers, *IEEE Trans. Magn.* **47**, 3036 (2011).
- [56] P. E. Blöchl, Projector augmented-wave method, *Phys. Rev. B* **50**, 17953 (1994).
- [57] J. P. Perdew, A. Ruzsinszky, G. I. Csonka, O. A. Vydrov, G. E. Scuseria, L. A. Constantin, X. Zhou, and K. Burke, Restoring the density-gradient expansion for exchange in solids and surfaces, *Phys. Rev. Lett.* **100**, 136406 (2008).